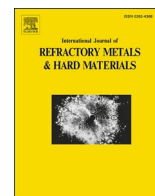




Contents lists available at ScienceDirect

# International Journal of Refractory Metals and Hard Materials

journal homepage: [www.elsevier.com/locate/IJRMHM](http://www.elsevier.com/locate/IJRMHM)

## Insights into microstructural evolution of tungsten-tungsten carbide plasma facing composite materials prepared by field assisted sintering technique

Aljaž Iveković<sup>a,\*</sup>, Matej Kocen<sup>a,b</sup>, Petra Jenuš<sup>a</sup>, Anže Abram<sup>a</sup>, Črtomir Donik<sup>c</sup>, Saša Novak<sup>a,b</sup>

<sup>a</sup> Department for Nanostructured Material, Jožef Stefan Institute, Ljubljana, Slovenia

<sup>b</sup> Jožef Stefan International Postgraduate School, Ljubljana, Slovenia

<sup>c</sup> Department of Physics and Chemistry of Materials, Institute of Metals and Technology, Lepi pot 11, 1000 Ljubljana, Slovenia

### ARTICLE INFO

#### Keywords:

Tungsten  
Tungsten carbide  
Interface  
Microstructure  
Fusion energy

### ABSTRACT

Combining a stable, resilient W-W<sub>2</sub>C or WC as plasma-facing material, with thermally more conductive and ductile W as a structural material, may provide a solution for the demanding environment in the fusion reactor chamber. In order to ensure the structural stability of such layered composite, their phase composition and thermal stability at elevated temperatures and cyclic heat loads needs to be evaluated.

In situ densification and joining of W and W-xWC materials have been performed by field-assisted sintering technique. Microstructural analysis revealed that the interface layer formed between W and pure WC consists primarily of large W<sub>2</sub>C grains. Initially, equiaxed W<sub>2</sub>C grains are formed following the decarburisation of WC due to the large C concentration gradient. Further C diffusion results in the formation of larger anisotropic grains growing preferentially in the (0001) direction. A similar microstructure was observed when joining WC-reinforced W (W-xWC, x = 7, 17, 28, 33 at. % C) with WC. On the other hand, the joining of W with WC-reinforced W resulted in a sound joint with no observable grain growth at the interface, even at large C concentrations (e.g. 28 at. %). As formed, microstructures were stable after thermal ageing at 1600 °C for 24 h with no observable change in major microstructural features.

The combination of WC-reinforced W as high strength plasma facing armour material and W-structural material offers a promising composite solution for improved thermal stability under high cyclic heat loads expected in future fusion power plants.

### 1. Introduction

Tungsten has been considered the most suitable material for the divertor – the most thermally loaded part of the fusion reactor chamber, exposed to high energy thermal shocks and temperatures well above 1000 °C. Its high melting temperature, high thermal conductivity, low sputtering yield and relatively low activation regarding long-term waste management make it an ideal candidate for the most severe conditions. However, at high temperatures, pure tungsten (W) recrystallises, which results in the deterioration of its mechanical properties [1]. When exposed to high heat flux conditions, which are expected in future fusion power plants, recrystallisation of the plasma-facing surface is unavoidable. Furthermore, due to the continuous cyclic loading of the recrystallised surface cracks are formed due to plastic low cycle fatigue [1,2]. Further research is therefore needed to improve the stability of the plasma-facing material.

Binderless WC possesses specific advantageous properties in comparison to W [3]. It does not suffer from recrystallisation-induced softening, which makes it an attractive candidate for long-term use at high temperatures. Furthermore, it was demonstrated by Humphry-Baker et al. [4] that WC outperforms pure W when exposed to high-heat flux conditions, especially in contrast to tungsten in a recrystallised state. The authors concluded that the higher thermal shock performance found in WC compared to pure tungsten results from its higher strength at elevated temperatures (Table 2).

Alternatively, recently introduced W-W<sub>2</sub>C composites [5,6] are thermally stable and exhibit promising stability under high heat flux conditions. These composites are synthesised by mixing W powder with a carbon precursor, which reacts during sintering with tungsten to form W<sub>2</sub>C. Using different precursors [6] it has been established that WC nanoparticulate powder as the source of carbon and consolidation by field-assisted sintering (FAST) results in W-W<sub>2</sub>C composites with

\* Corresponding author.

E-mail address: [aljaz.ivekovic@ijs.si](mailto:aljaz.ivekovic@ijs.si) (A. Iveković).

<https://doi.org/10.1016/j.ijrmhm.2023.106301>

Received 8 November 2022; Received in revised form 1 June 2023; Accepted 12 June 2023

Available online 15 June 2023

0263-4368/© 2023 The Authors. Published by Elsevier Ltd. This is an open access article under the CC BY-NC-ND license (<http://creativecommons.org/licenses/by-nc-nd/4.0/>).

favourable mechanical properties at room and elevated temperatures. In contrast, prolonged ageing at 1600 °C has only a minor effect [5]. The study by Novak et al. [5] revealed that carbon content significantly impacts the microstructure of the W-W<sub>2</sub>C composites and their mechanical and thermophysical properties.

Table 1 summarises the basic thermo-physical properties of baseline tungsten material in its as-produced (hot rolled and forged) and recrystallised state, as well as the properties of tungsten carbides and tungsten carbide, reinforced tungsten composite (W-W<sub>2</sub>C).

Although binderless tungsten carbides and carbide-reinforced tungsten composites are promising as plasma-facing armour material, their brittleness limits their use as a stand-alone structural material. A stable, resilient W-W<sub>2</sub>C or WC as plasma-facing material, with thermally more conductive and ductile W as a structural material, may provide a solution for the demanding environment in the fusion reactor chamber. Carbide surface coatings can be produced by CVD, PVD or carburisation of W surface [10,11]; however, there is limited literature on the phase composition of these layers and their thermal stability at elevated temperatures and cyclic heat loads.

According to the W–C phase diagram, a small solid solubility of C in W exists, attaining a maximum of 0.3 at. % C at the eutectic temperature of about 2400 °C [12]. The solubility of C in W decreases rapidly with temperature to 0.05 at. % of C near 2000 °C and to trace amounts at lower temperatures. Below 1500 °C, W<sub>2</sub>C precipitates appear stable against the W matrix [13]. However, there is a lack of knowledge on the decarburisation of WC in the presence of W, the consequential formation of the lower W<sub>2</sub>C phase and its stability against the W matrix.

The diffusion of C in the W–C system has mainly been investigated in the context of tungsten carburisation. Carburisation of W is initiated by forming a thin layer of WC at the surface. Subsequently, starting from the WC layer, the tungsten metal gradually converts to W<sub>2</sub>C. The initial fast formation of W<sub>2</sub>C is followed by a much slower conversion of W<sub>2</sub>C into WC until the carburisation reaction to WC is finished [14]. Specific diffusion data for C in W is scarce, mainly limited to high temperatures and low C concentrations. Literature values of diffusion of carbon in metallic tungsten range from  $9 \times 10^{-8} \text{ cm}^2\text{s}^{-1}$  at 1500 °C to  $4.5 \times 10^{-6} \text{ cm}^2\text{s}^{-1}$  at 2400 °C, with activation energies between 37.8 and 53.5 kcal·mol<sup>-1</sup>, depending on temperature, tungsten quality, and method of measurement [15].

Schmid and Roth [16] investigated the diffusion of carbon over a wide range of concentrations in the temperature range between 1000 and 1100 K. They concluded that the diffusion of C in W depends strongly on the carbon concentration and temperature. Maximum diffusion was determined at low C concentrations ( $10^{-15}$ – $10^{-14} \text{ cm}^2\text{s}^{-1}$ , at C concentration below 15%) with a sharp drop of approximately one order of magnitude at C concentrations corresponding to the C concentration in W<sub>2</sub>C and WC. Lower diffusion of carbon at high concentrations was attributed to the negligible diffusion coefficient of carbon in W<sub>2</sub>C and WC in the considered temperature range. At higher temperatures, the diffusion coefficients for carbon in W<sub>2</sub>C were reported as  $8.1 \times 10^{-10} \text{ cm}^2\text{s}^{-1}$  at 1526 °C, and  $5 \times 10^{-6} \text{ cm}^2\text{s}^{-1}$  at 2400 °C, with respective activation energy between 100 and 111 kcal·mol<sup>-1</sup> [15].

The aim of this work was to get a better understanding of carbon

diffusion in the W-WC system. Due to the sensitivity of microstructure and physicochemical properties of these materials to carbon content, an understanding of carbon diffusion and resulting phase composition is needed to assume the stability of the potential layered structure. Therefore, in this study, we investigated the formation and the stability of microstructures in diffusion couples between WC, W-W<sub>2</sub>C and W, co-sintered using field-assisted sintering and during ageing at relevant operating temperatures.

## 2. Materials and methods

In this study, tungsten powder with grain size  $\leq 1.5 \mu\text{m}$  (Global Tungsten & Powders spol. S r.o., Czech Republic) and tungsten carbide (WC) with grain size 150–200 nm (>99%, Aldrich, Germany) were used. According to the producer's specification, the oxygen content in the powders was 0.16 wt% (1.8 at. %) and 0.2 wt% (2.4 at. %), respectively. In the case of powder mixtures, W and WC powders were mixed in cyclohexane suspension (Sigma Aldrich, Germany), and any possible agglomerates were broken with an ultrasonic processor VCX500 (Sonic & Materials Inc., USA) for 3 min at a power of 250 W, frequency 20 kHz and pulse on/off of 1 s. WC milling balls (diameter 1 cm) were added to the mixture in the powder-to-balls ratio of 1:1 and mixed in a shaker-mixer (Turbula T2F, WAB, Germany) for 24 h. The suspension was frozen with liquid nitrogen to prevent uneven sedimentation of the powders with different grain sizes and later freeze-dried using a lyophilisator (Alpha 2–4 LDplus, CHRIST, Germany).

Diffusion couples were prepared by subsequently cold pressing layers of W and WC powders in different ratios ranging from pure W to pure WC. First powder composition was poured into the graphite die and compacted with 50 MPa of pressure, afterward the second powder was added and the entire die setup was compacted again. The exact composition of various powder mixtures and resulting W<sub>2</sub>C content after densification are collected in Table 2. Sintering was performed in a graphite die with an inner diameter of 10 mm using field-assisted sintering (FAST, SPS, Dr. Sinter FAST 515-S, Sumimoto FAST Syntex Ltd., Japan) in a vacuum at 1900 °C with a heating rate of 100 °C/min, for 5 min and applied uniaxial pressure of 60 MPa. Before the FAST processing, the reaction chamber was purged twice with high-purity argon (min. Purity 99.999%) and evacuated again. During sintering, the pressure inside the chamber was below 10 Pa.

**Table 2**  
Composition of individual layers.

Sample	wt% of WC in the powder mixture	at. % of C in the powder mixture*	Densification	wt% of W <sub>2</sub> C in sintered material
W	0	0		0
W7WC	8	7		7
W17WC	21.1	17	1900 °C,	32
W28WC	40.4	28	5 min,	70
W33WC	51.6	33	60 MPa	99
WC	100	50		4

\* calculated based on the wt% of added WC powder.

**Table 1**

Basic thermophysical properties of as-produced W (hot rolled and forged), recrystallised W (W<sub>rx</sub>) [7]; WC, W<sub>2</sub>C [8,9] and W-W<sub>2</sub>C (7 at. % C in initial powder mixture) composite material [5].

	Density	Melting temperature	Hardness	Fracture strength		Thermal conductivity	
	gcm <sup>-3</sup>	°C	GPa	MPa		Wm <sup>-1</sup> K <sup>-1</sup>	
				RT	1000 °C	RT	1000 °C
W	19.25	3425	4.3	785	335	164	116
W <sub>rx</sub>	19.25	3425	3.5	203	86	164	116
WC	15.7	2800	25.5	NA	1107	110	71
W <sub>2</sub> C	17.2	2730	19.6	NA	757	12	33
W7WC (7 at. % C)	19.1	N/A	5.1	896	823	127	103

In select experiments, small amount of  $Y_2O_3$  powder (99.9%, 50–70 nm, Alfa Aesar, Germany) was deposited between layers in order to determine the initial position of the interface between pressed powders.

To estimate the effect of ageing (prolonged heating) on the microstructure, sintered samples were subsequently heated at 1600 °C for 24 h in a high-temperature vacuum furnace (Thermal Technology, USA).

Microstructures were examined on grinded and polished cross-sections using scanning electron microscopy (FE-SEM, JSM-7600F, Jeol Inc.). In addition, EBSD analyses were performed on a ZEISS FIB-SEM CrossBeam 550 (Carl Zeiss AG, Oberkochen, Germany) with an EDAX Hikari super EBSD Camera (Ametek Inc., Bervyn, PA, USA). The EBSD used a 70° tilt angle with an acceleration voltage of 15 kV and a probe current of up to 10 nA, with working distance of 18 mm. Step size ranged from 0.2 to 1  $\mu\text{m}$  depending on the used magnification and sample grain size. EBSD data was analysed using EDAX OIM Analysis 8.6 post processing software.

### 3. Results and discussion

#### 3.1. W-WC

A polished cross-section of the sintered W-WC diffusion couple is presented in Fig. 1. During sintering, an approximately 100  $\mu\text{m}$  thick diffusion layer was formed, composed of three distinct layers (Fig. 1a). Large uniaxial grains oriented perpendicular to the interface were observed close to W and WC, with smaller equiaxed grains in between. The layer of uniaxial grains closer to tungsten is slightly smaller than those closer to WC. Moreover, a 30  $\mu\text{m}$  thick porosity layer is observed in the transition layer of uniaxial grains in the proximity of W. The porosity level and pore size, which resemble the porosity observed in W, indicate that the formation of uniaxial grains followed the initial densification of W. Residual porosity in W layer is the result of W-oxide formation from oxygen impurities during sintering which hinders further densification [5,17].

Along the grain boundaries of uniaxial grains within the porous layer, thin secondary phase grains were also observed (Fig. 1b). Similar grains were not observed at the grain boundaries of similar grains closer to WC.

Additionally, multiple microcracks were observed perpendicular to the interface and sometimes extending into the WC layer. The formation of cracks is most likely the result of stress accumulation due to the differential densification of W and WC. Zeiler et al. [18] and Oliphant et al. [19] observed extensive cracking of the carbide layer during the carburisation of W wire. The formation of cracks was ascribed to the incorporation of C in the lattice, the filament's subsequent volume expansion, and the differences in density between W and its carbides that induce tension in the carbide layer.

To determine the initial position of the interface between W and WC,

$Y_2O_3$  powder was introduced at the interface to serve as an inert marker (Fig. 2). Fine  $Y_2O_3$  dispersions are often used to reinforce tungsten, due to their thermodynamic stability [20]  $Y_2O_3$  remained stable, and no reaction with W or WC was observed.

The position of  $Y_2O_3$  particles after densification implies that the initial interphase was located at the border of the porous layer and not in the centre of the diffusion layer, where smaller equiaxed grains were present. Based on this observation, it is speculated that the equiaxed grains nucleated first due to C diffusion from WC toward W. Following the initial nucleation of equiaxed grains, uniaxial grains proceeded to grow in both directions, as depicted in Fig. 3.

Microhardness measurements were also performed across the layers. We observed low hardness of approximately 4.9 GPa (500  $HV_{10}$ ) on the W side, which indicates the presence of pure W. Abrupt increase in hardness was observed in the porous layer of elongated grains, where it reached a value of 14.5–15.7 GPa (1480–1600  $HV_{10}$ ). The hardness of the equiaxed and elongated grains without porosity increased to 18.1–18.6 GPa (1850–1900  $HV_{10}$ ), which is in the range of hardness of  $W_2C$  phase. Considering the effect of porosity on hardness, also the elongated grains where the porosity is present could be attributed to  $W_2C$  [8]. At the WC side, a further increase in hardness up to 24.5 GPa (2500  $HV_{10}$ ) was observed, indicative of the presence of pure WC.

As the microstructural determination of phase composition in the W–C system is a challenging task due to the low contrast difference between tungsten and its carbides, the composition of the diffusion zone was further analysed by EBSD, which confirmed the presence of a diffusion layer consisting predominantly of  $W_2C$  grains (Fig. 4).  $W_2C$  grain growth, presumably initiated from the initial equiaxed grains, continues preferentially in the  $\langle 0001 \rangle$  direction (Fig. 4c). Poor indexation in the WC layer results from the significantly smaller grain size. Therefore, additional EBSD maps at higher magnification and sufficiently small step size were performed on the W- $W_2C$  (Fig. 5) and  $W_2C$ -WC (Fig. 6) boundaries.

A detailed EBSD map at the boundary between the W and  $W_2C$  layer revealed that the thin grains located at the grain boundaries between uniaxial  $W_2C$  grains are the remnant W (Fig. 5). Small W grains were also observed within the  $W_2C$  grains, predominantly situated next to the pores (black dots). As the carbon atoms are located in the interstices between the metal atoms, the diffusion of carbon in tungsten and its carbides proceeds via a vacancy mechanism rather than grain boundaries [15]. As a result, such diffusion mechanism could explain the presence of residual W grains located at the grain boundaries and pores. The presence of these W-grains coincides with the layer of porosity observed in the vicinity of the W layer (Fig. 1a), additionally corroborating the speculation that the formation of  $W_2C$  grains followed the initial densification of W.

The transition between  $W_2C$  and WC (Fig. 6) is more straightforward, with an abrupt structure and phase composition change. Small  $W_2C$

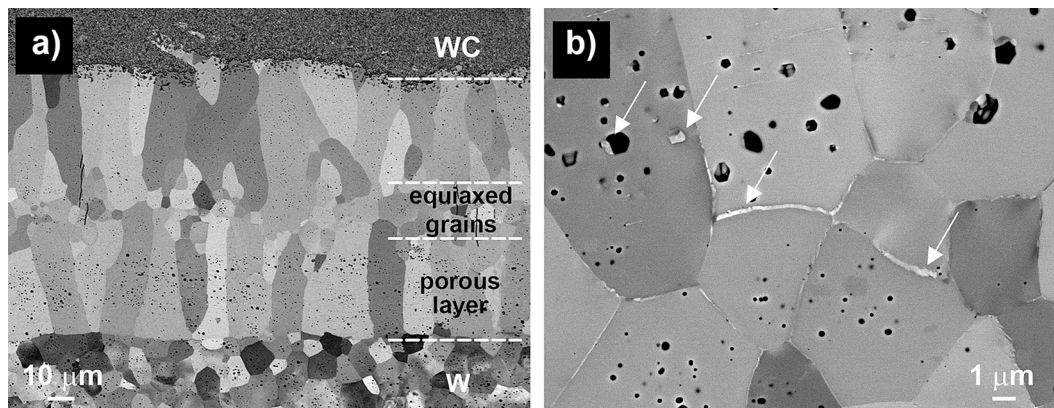


Fig. 1. SEM image of a) complete diffusion couple between W and WC (a) and porosity and secondary phase between elongated grains (marked with arrows).

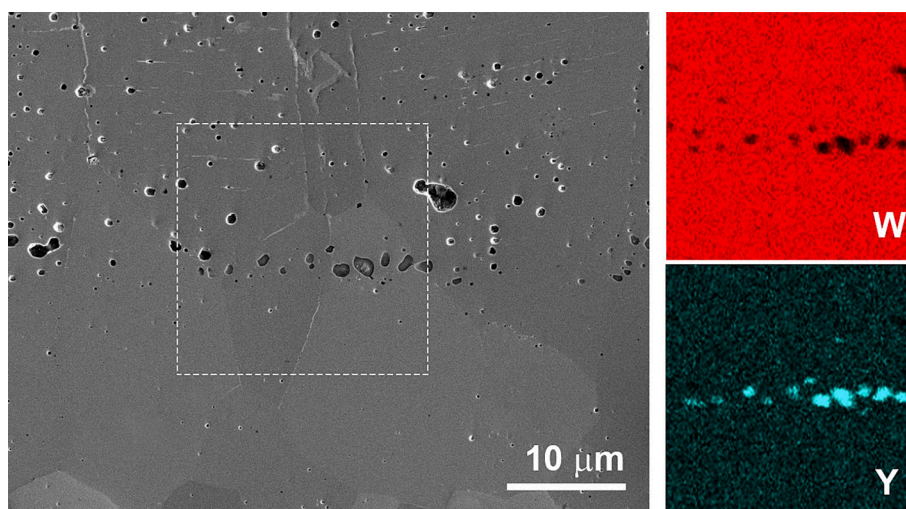


Fig. 2. SEM image of the initial interface marked by  $Y_2O_3$  particles and corresponding EDXS mapping of the marked area.

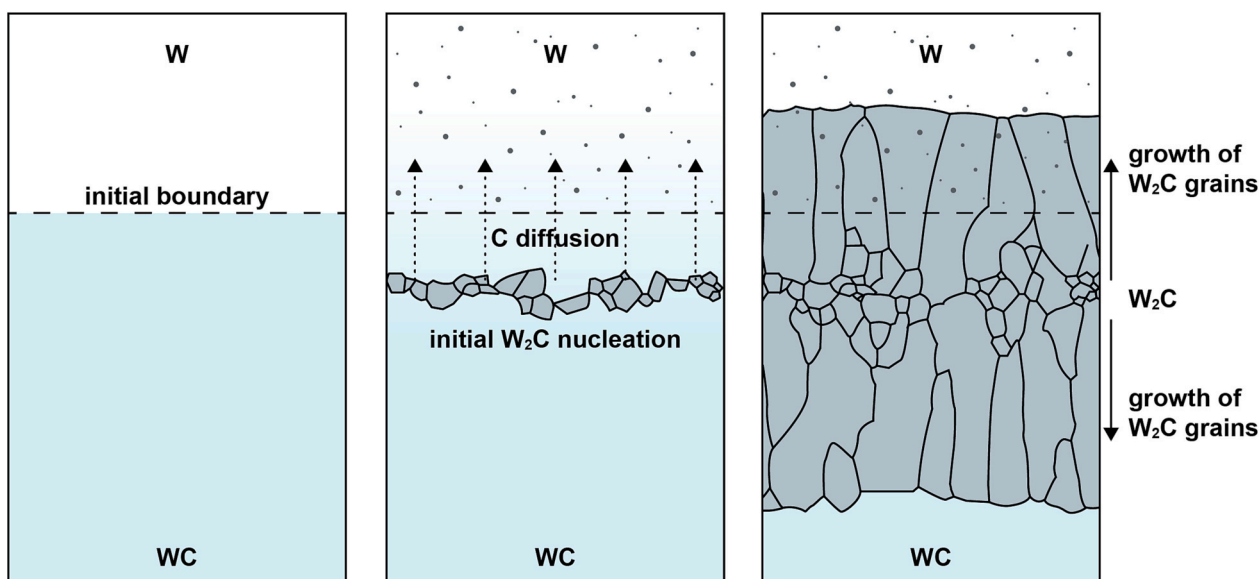


Fig. 3. Schematic representation of the formation of the interphase layer between W and WC.

grains are observed within the WC layer, which is typical for the densification of WC without the addition of free carbon [21].  $W_2C$  is formed due to the high-temperature reaction of WC with oxide passivation layers at the surface of WC grains.

### 3.2. WC-(W- $W_2C$ )

To investigate the effect of the C gradient on the formation of the interface layer between the W and WC, diffusion couples between various W-WC powder mixtures with varying C content (7, 17 or 33 at. % C in the initial powder mixture) and WC were prepared and evaluated. Fig. 7 presents the interphase between WC and samples W7WC and W17WC (containing 7 and 17 at. % carbon, respectively). In both cases, a similar interphase layer is observed as in the case of pure W and WC diffusion couple, with a total width of the diffusion zone of 100  $\mu m$  and 140  $\mu m$ , respectively. However, there is a noticeable difference in the size of the uniaxial grains and the position of the equiaxed grains, which are located closer to the WC side of the diffusion couple (Fig. 7). The difference in the position of equiaxed grains can be ascribed to the higher C content (7 and 17 at.% respectively) in the initial powder

mixture in contrast to pure W and thus faster formation of initial  $W_2C$  grains. In line with previous experiments, microcracking of the  $W_2C$  layer perpendicular to the interphase was also observed.

Conversely, with 33 at. % C, the composition which results in the formation of pure  $W_2C$  after densification, the transition layer between the two carbides, consists of a mixture of both phases, with large WC grains within the  $W_2C$  matrix (Fig. 8)

### 3.3. Gradient transition

As was demonstrated above, the formation of the  $W_2C$  layer cannot be eliminated in contact with WC; however, the stresses during densification might be mitigated by introducing a gradual transition between W and its carbides. Various samples with gradient microstructure ranging from W to WC with intermediate layers of W-xWC with 7, 17, 28, 33 at. % of carbon were prepared (Fig. 9), and individual transition layers were investigated.

In contrast to the W-WC diffusion couple, no grain growth and formation of a distinct reaction layer was observed between W and carbide-reinforced W composites (W-xWC,  $x = 7, 17$  and 28 at. % of C), but

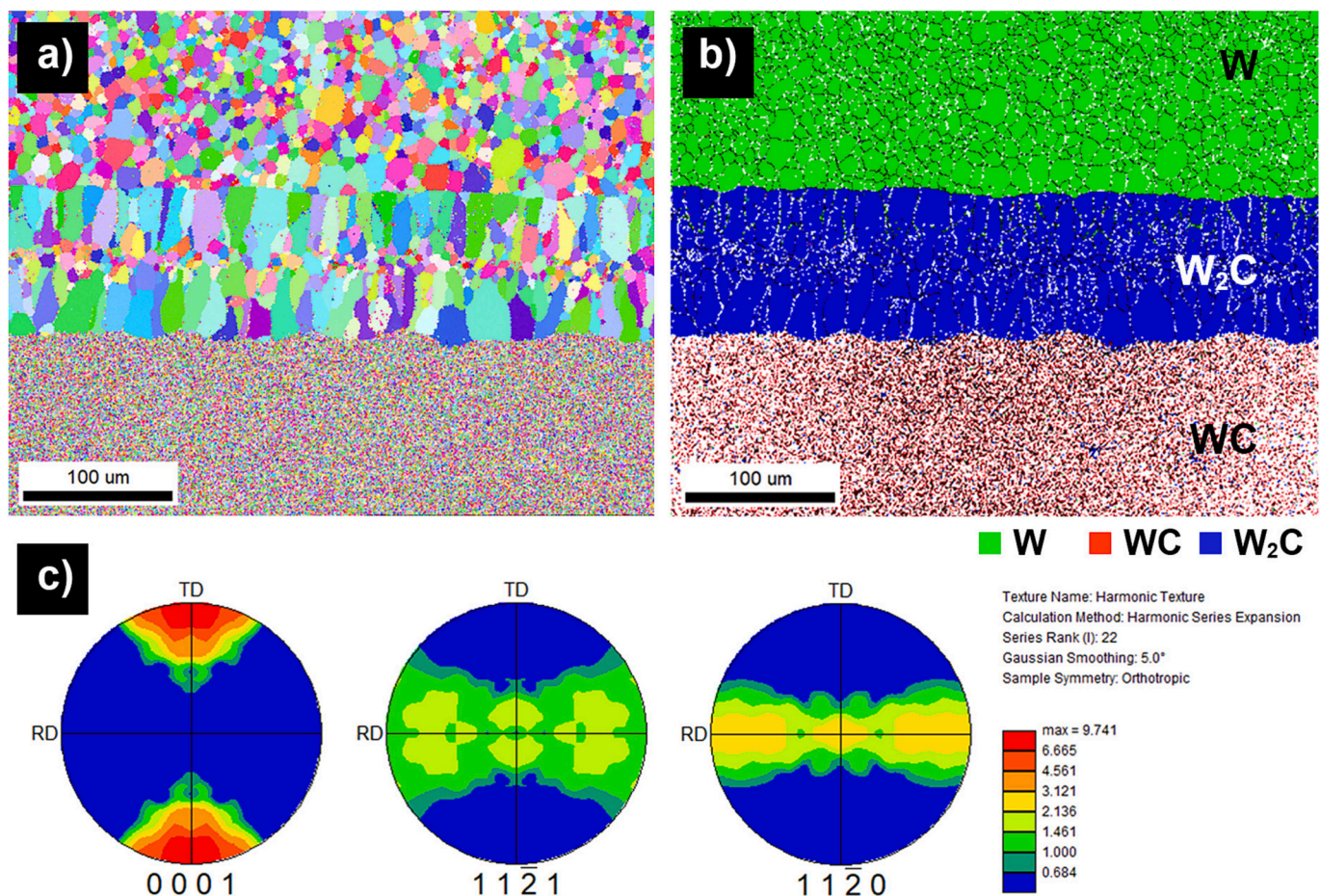


Fig. 4. a) EBSD inverse pole figure in Z direction (IPF Z) of the entire diffusion zone, b) respective phase distribution by colour; W - green, WC - red, W<sub>2</sub>C - blue and c) pole figure representation of W<sub>2</sub>C grains. (For interpretation of the references to colour in this figure legend, the reader is referred to the web version of this article.)

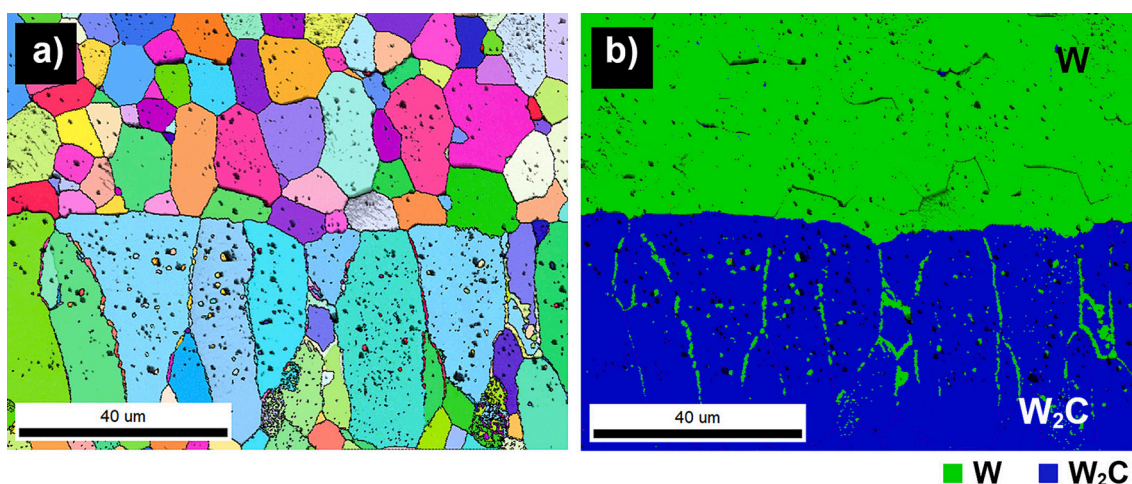


Fig. 5. a) EBSD inverse pole figure in Z direction (IPF Z) of W-W<sub>2</sub>C boundary and b) its respective phase distribution by colour; W - green, W<sub>2</sub>C - blue. (For interpretation of the references to colour in this figure legend, the reader is referred to the web version of this article.)

rather a coherent, clear transition between W and carbide-reinforced composites (Fig. 10). Surprisingly, even layers with high C content (W28WC) didn't exhibit any reaction layer or excessive grain growth at the interface (Fig. 10b).

As previously described [5], WC particles react with the W matrix to form W<sub>2</sub>C particles located at the grain boundaries. Without an

additional carbon source (e.g. WC), W<sub>2</sub>C appears stable against W. As was suggested by Schmidt and Roth [16] the diffusion of C in W is highly dependent on concentration and is retarded at compositions corresponding to the C concentration in W<sub>2</sub>C and WC, therefore limiting further diffusion and ripening. Although most of the intermediate layers appeared well-defined without any elongated grains, the transition

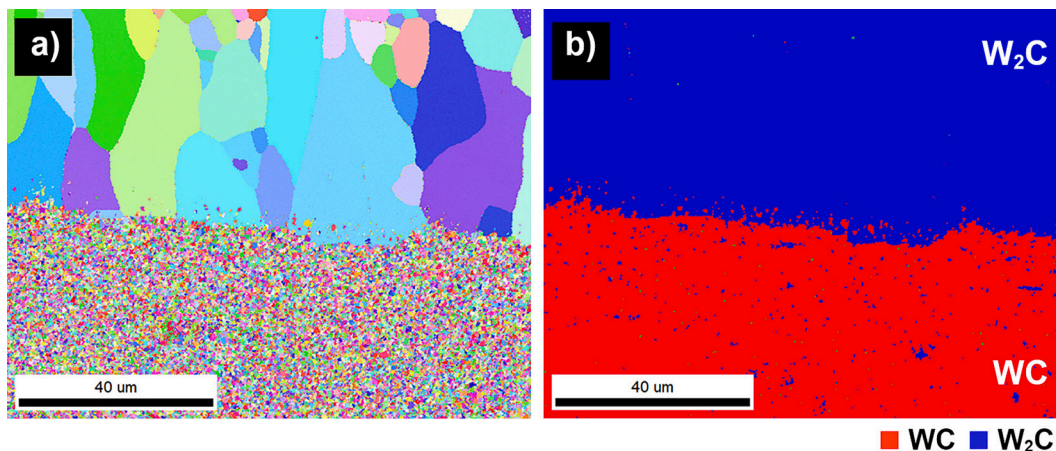


Fig. 6. a) EBSD inverse pole figure in Z direction (IPF Z) of W<sub>2</sub>C-WC boundary and b) its respective phase distribution by colour; W<sub>2</sub>C – blue, WC – red. (For interpretation of the references to colour in this figure legend, the reader is referred to the web version of this article.)

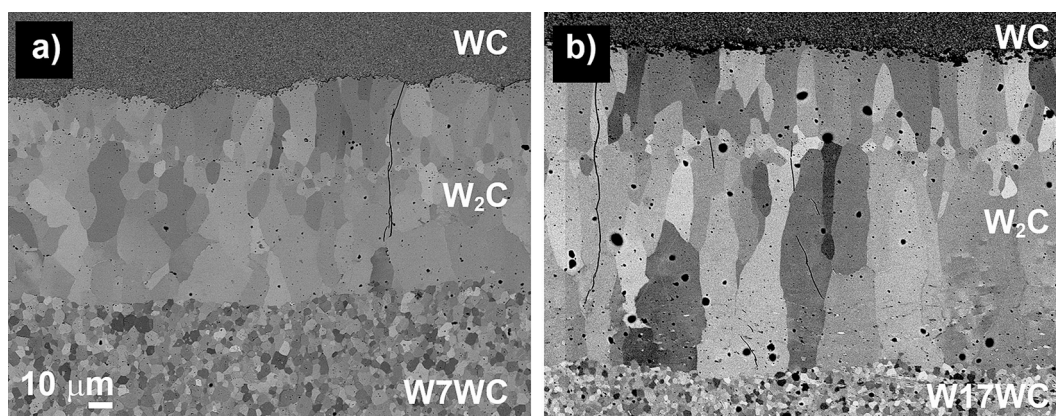


Fig. 7. Diffusion layer between a) WC and W7WC and b) WC and W17WC.

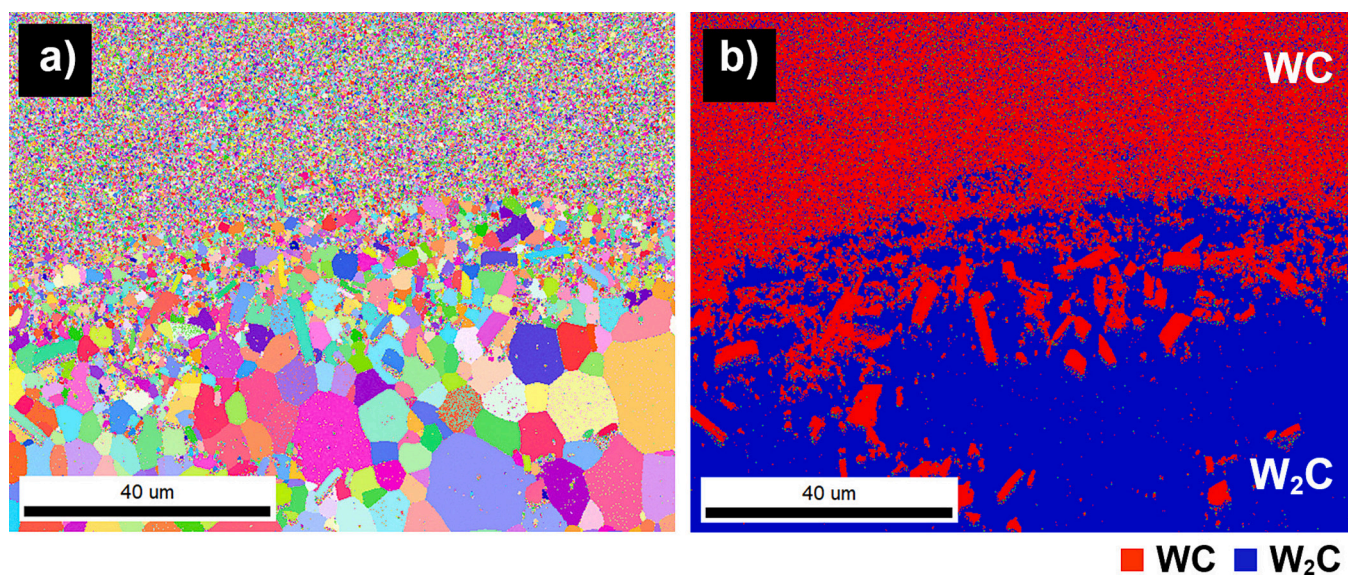


Fig. 8. a) EBSD inverse pole figure in Z direction (IPF Z) of diffusion layer between WC and W33WC and b) its corresponding EBSD phase map by colour; W<sub>2</sub>C – blue, WC – red. (For interpretation of the references to colour in this figure legend, the reader is referred to the web version of this article.)

between W33WC (~W<sub>2</sub>C) and layers with less C (e.g. W28WC, W17WC) still resulted in grain growth at the interface. The EBSD analysis of the interface between W33WC and W28WC is presented in Fig. 11. The

transition layer, with a thickness between 25 and 30 μm, consisted of larger W<sub>2</sub>C grains.

The results suggest that a combination of a carbide-reinforced

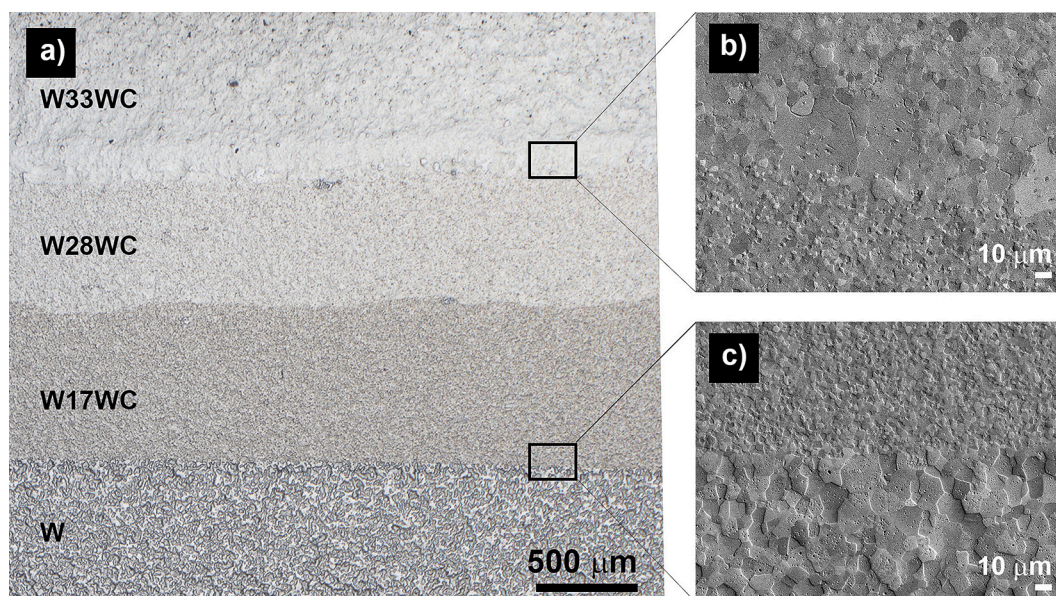


Fig. 9. Optical micrograph of a sample with a) a gradient in composition ranging from W-W17WC-W28WC-W33WC.

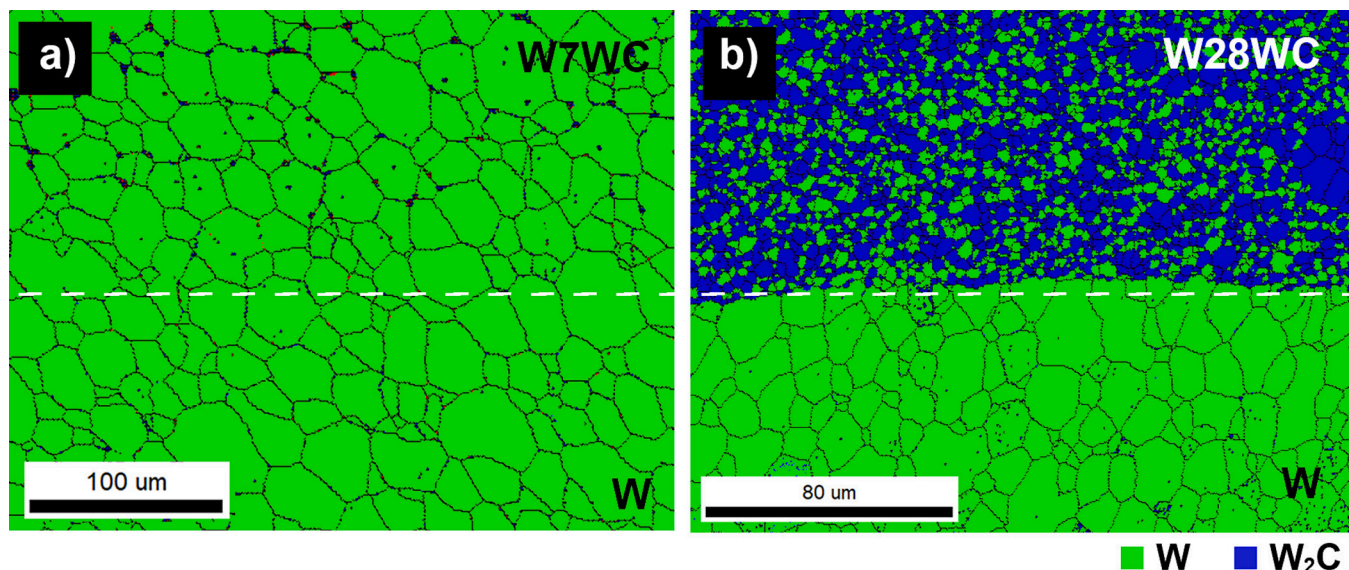


Fig. 10. EBSD phase distribution map by the colour of the interphase between a) W and W7WC and b) W and W28WC.

tungsten (W-xWC) layer and pure W can be successfully fabricated without an observable interaction layer or the formation of cracks at the interface. Furthermore, the control over the amount of carbide reinforcement offers the ability to optimise the balance between high strength and thermal conductivity to maximise the component's thermal shock resistance.

### 3.4. Ageing

Thermal stability of the formed interphases is crucial to ensure the stability of the component. Exact operating temperature window of the divertor is difficult to define. The heat load on the divertor surface is predicted to reach  $10 \text{ MW/m}^2$  during quasi-stationary operation and up to  $20\text{--}40 \text{ MW/m}^2$  during slow transient events (1–10 s) [22]. The expected surface temperature during steady state operation will reach  $1000 \text{ }^\circ\text{C}$ , however during slow transient events and/or plasma disruptions the temperature will rise up to  $2000 \text{ }^\circ\text{C}$  and beyond [23]. To examine the stability of the formed interfaces, ageing heat treatment

was performed at an arbitrary value of  $1600 \text{ }^\circ\text{C}$  in vacuum for 24 h. Following the heat treatment, the microstructure of the selected interphase was re-examined and compared to the as sintered one. The thickness of the diffusion layer remained unchanged (Fig. 12a) and all of the initial microstructural features, such as thin W grains at the  $\text{W}_2\text{C}$  grain boundaries (Fig. 12b), were still observed. Similar observations were made on gradient samples after ageing.

Additionally, EBSD analysis of the interphase confirmed that the diffusion layer of  $\text{W}_2\text{C}$  grains remained unaltered, with  $\text{W}_2\text{C}$  grains oriented preferentially in the  $\langle 0001 \rangle$  direction (Fig. 13). Analysis of the grain size of  $\text{W}_2\text{C}$  grains revealed a slight increase in the mean grain size value from  $6.9 \pm 5.9 \text{ } \mu\text{m}$  in the as-sintered state to  $8.1 \pm 6.3 \text{ } \mu\text{m}$  in the annealed state. Furthermore, the grain misorientation angle decreased from  $37.92^\circ$  to  $35.75^\circ$  in the as-produced and annealed state respectively.

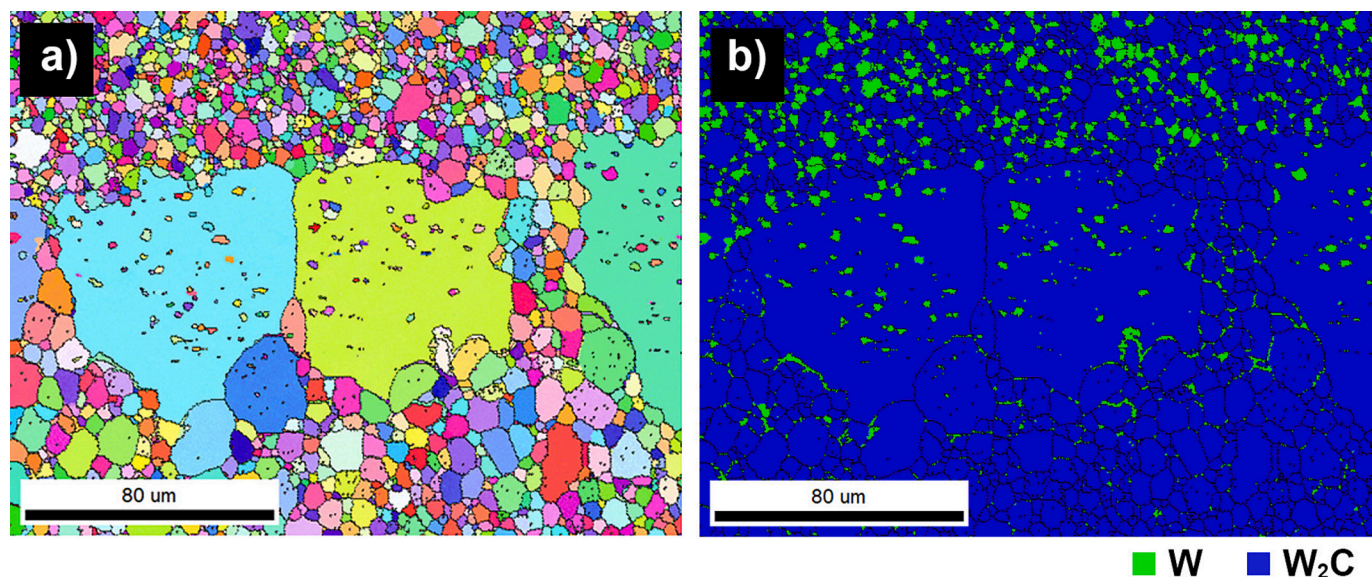


Fig. 11. a) EBSD inverse pole figure in Z direction (IPF Z) of the boundary between samples W28WC and W33WC and b) its respective phase distribution by colour; W – green, W<sub>2</sub>C – blue. (For interpretation of the references to colour in this figure legend, the reader is referred to the web version of this article.)

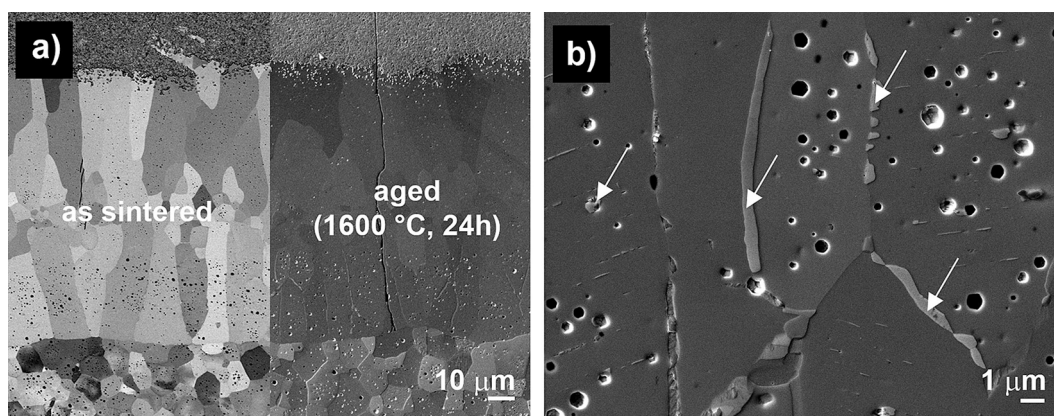


Fig. 12. a) Comparison of the W<sub>2</sub>C layer thickness between W and WC in the sintered stage and after thermal ageing and b) W grains at the W<sub>2</sub>C grain boundaries after ageing.

#### 4. Conclusions

The possibility of joining WC- or W<sub>2</sub>C-reinforced W with W by simultaneously sintering layers of powder mixtures by field assisted sintering has been studied. The effect of C concentration on the formation of a reaction layer and its stability has been analysed utilising electron microscopy and EBSD.

The results suggest that in-situ densification and joining of W and WC results in a 100 μm interaction layer consisting predominantly of W<sub>2</sub>C grains. Initially, equiaxed W<sub>2</sub>C grains are formed following the decarburisation of WC due to the large C concentration gradient. Further C diffusion results in the formation of larger anisotropic grains growing preferentially in the <0001> direction. The resulting W<sub>2</sub>C layer acts as a thermal barrier, which is not desirable in high-heat-flux applications, where efficient heat transfer is required. Furthermore, differential densification of W and WC results in microcracks perpendicular to the interphase, which further deteriorates the properties of the formed joint. By decreasing the C gradient and joining WC with carbide-reinforced W (W-xWC) did not prevent or limit the formation of the interface layer. The thickness of the interface layer increased with higher C concentration in the W-xWC layer.

To mitigate the stresses during densification and avoid the excessive

W<sub>2</sub>C grain growth, we proposed and evaluated a stepwise gradual phase transition. By stacking layers with varying C content, a gradient microstructure was realised, with a coherent transition from W to carbide-reinforced W-composite with high W<sub>2</sub>C concentration, without observable grain growth or formation of cracks. Once W<sub>2</sub>C grains are formed, they are stable against W-matrix and no further diffusion or grain growth was observed even for high concentration of carbides. Microstructures of the formed joints remained unchanged even after high temperature ageing at 1600 °C for 24 h.

The presented results support the hypothesis that gradient composite with W-core and carbide-reinforced W plasma-facing surface could potentially offer a composite material solution for components exposed to high cyclic heat loads in a nuclear fusion reactor. In future work, the assessment of low cycle thermal fatigue, via transient heating events up to 20 MW/m<sup>2</sup>, should be performed and evaluated.

#### CRediT authorship contribution statement

**Aljaž Iveković:** Conceptualization, Methodology, Writing – original draft. **Matej Kocen:** Investigation. **Petra Jenuš:** Conceptualization, Methodology. **Anže Abram:** Visualization. **Črtomir Donik:** Visualization, Investigation. **Saša Novak:** Supervision.

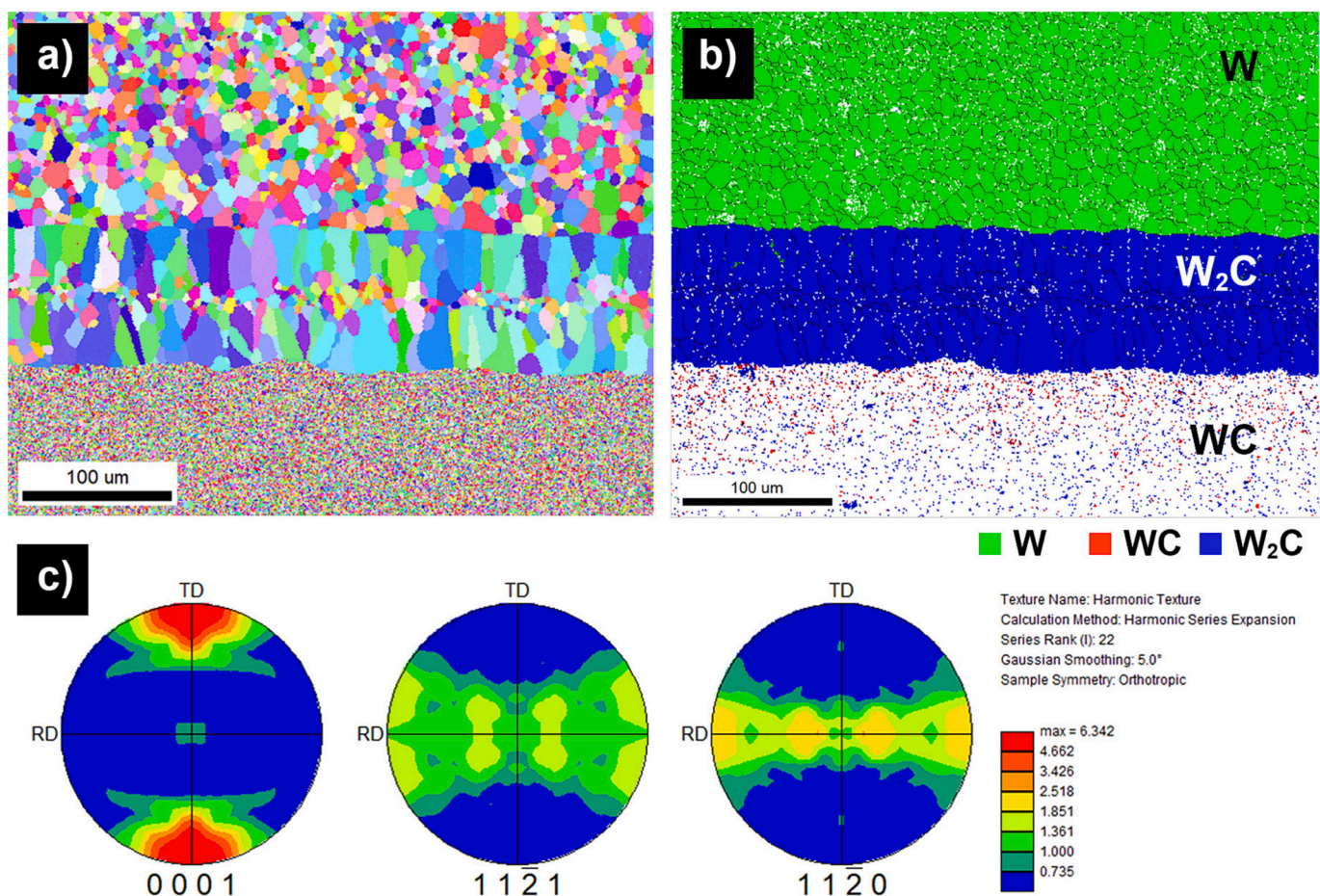


Fig. 13. a) EBSD inverse pole figure in Z direction (IPF Z) of the entire diffusion zone after annealing at 1600 °C for 24 h, b) respective phase distribution by colour; W - green, WC - red, W<sub>2</sub>C - blue and c) pole figure representation of W<sub>2</sub>C grains. (For interpretation of the references to colour in this figure legend, the reader is referred to the web version of this article.)

### Declaration of Competing Interest

The authors declare that they have no known competing financial interests or personal relationships that could have appeared to influence the work reported in this paper.

### Data availability

Data will be made available on request.

### Acknowledgement

This work has been carried out within the framework of the EUROfusion Consortium, funded by the European Union via the Euratom Research and Training Programme (Grant Agreement No 101052200 — EUROfusion). Views and opinions expressed are however those of the author(s) only and do not necessarily reflect those of the European Union or the European Commission. Neither the European Union nor the European Commission can be held responsible for them.

### References

- G. Pintsuk, et al., Qualification and post-mortem characterization of tungsten mock-ups exposed to cyclic high heat flux loading, *Fus. Eng. Design* 88 (9) (2013) 1858–1861.
- M. Li, J.-H. You, Interpretation of the deep cracking phenomenon of tungsten monoblock targets observed in high-heat-flux fatigue tests at 20MW/m<sup>2</sup>, *Fus. Eng. Design* 101 (2015) 1–8.
- S.A. Humphry-Baker, G.D.W. Smith, Shielding materials in the compact spherical tokamak, *Philos. Trans. R. Soc. A Math. Phys. Eng. Sci.* 377 (2141) (2019) 20170443.
- S.A. Humphry-Baker, G.D.W. Smith, G. Pintsuk, Thermal shock of tungsten carbide in plasma-facing conditions, *J. Nucl. Mater.* 524 (2019) 239–246.
- S. Novak, et al., Beneficial effects of a WC addition in FAST-densified tungsten, *Mater. Sci. Eng. A* 772 (2020), 138666.
- P. Jenuš, et al., W<sub>2</sub>C-reinforced tungsten prepared using different precursors, *Ceram. Int.* 45 (6) (2019) 7995–7999.
- M. Gorley, et al., The EUROfusion materials property handbook for DEMO in-vessel components—status and the challenge to improve confidence level for engineering data, *Fus. Eng. Design* 158 (2020), 111668.
- G. Berg, et al., Data collection of properties of hard material, in: *Handbook of Ceramic Hard Materials*, 2000, pp. 965–995.
- E.M. Garcia-Ayala, et al., Thermomechanical behaviour of WC-W<sub>2</sub>C composites at first wall in fusion conditions, *Int. J. Refract. Met. Hard Mater.* 98 (2021), 105565.
- Z. Zhao, et al., A new strategy to efficiently fabricate tungsten carbide coating on tungsten: two-step interstitial carburization, *Surf. Coat. Technol.* 389 (2020), 125579.
- E. Quesnel, et al., Tungsten and tungsten-carbon PVD multilayered structures as erosion-resistant coatings, *Surf. Coat. Technol.* 62 (1) (1993) 474–479.
- H.J. Goldschmidt, J.A. Brand, The tungsten-rich region of the system tungsten-carbon, *J. Less Common Metals* 5 (2) (1963) 181–194.
- A.S. Kurlov, A.I. Gusev, Ordering of tungsten carbides, in: A.S. Kurlov, A.I. Gusev (Eds.), *Tungsten Carbides: Structure, Properties and Application in Hardmetals*, Springer International Publishing, Cham, 2013, pp. 57–108.
- G. Mühlbauer, et al., Transition of W<sub>2</sub>C to WC during carburization of tungsten metal powder, *Int. J. Refract. Met. Hard Mater.* 72 (2018) 141–148.
- E. Lassner, S. WD, *Important Aspects of Tungsten Chemistry*, in *Tungsten*, Springer, Boston, MA, 1999.
- K. Schmid, J. Roth, Concentration dependent diffusion of carbon in tungsten, *J. Nucl. Mater.* 302 (2) (2002) 96–103.
- A. Sestan, et al., Tungsten carbide as a deoxidation agent for plasma-facing tungsten-based materials, *J. Nucl. Mater.* 524 (2019) 135–140.
- E. Zeiler, et al., Structural changes of tungsten heating filaments during CVD of diamond, *Mater. Sci. Eng. A* 335 (1) (2002) 236–245.

- [19] C.J. Oliphant, et al., EBSD analysis of tungsten-filament carburization during the hot-wire CVD of multi-walled carbon nanotubes, *Microsc. Microanal.* 20 (1) (2014) 4–13.
- [20] M. Duerschnebel, et al., Elucidating the microstructure of tungsten composite materials produced by powder injection molding, *Nucl. Mater. Energy* 24 (2020), 100766.
- [21] J. Sun, et al., A review on Binderless tungsten carbide: development and application, *Nano-Micro Lett.* 12 (1) (2019) 13.
- [22] J.H. You, et al., High-heat-flux technologies for the European demo divertor targets: state-of-the-art and a review of the latest testing campaign, *J. Nucl. Mater.* 544 (2021), 152670.
- [23] J.H. You, et al., European DEMO divertor target: operational requirements and material-design interface, *Nucl. Mater. Energy* 9 (2016) 171–176.